1198 *Inorg. Chem.* **2010**, *49*, 1198–1205
DOI: 10.1021/ic9021728

Inorganic Chemistry
Article

Synthesis, Structures, and Multinuclear NMR Spectra of Tin(II) and Lead(II) Complexes of Tellurium-Containing Imidodiphosphinate Ligands: Preparation of Two Morphologies of Phase-Pure PbTe from a Single-Source Precursor

Jamie S. Ritch,[†] Tristram Chivers,*[,†] Kibriya Ahmad,[‡] Mohammad Afzaal,[‡] and Paul O'Brien[‡]

[†]*Department of Chemistry, University of Calgary, Calgary AB T2N 1N4, Canada and* [‡]*The School of Chemistry and The School of Materials, The University of Manchester, Oxford Road, Manchester M13 9PL, U.K.*

Received November 3, 2009

Group 14 metal complexes of heavy chalcogen-centered anions, $M[(TeP^iPr_2)_2N]_2$ (**5**, M = Sn; **6**, M = Pb) and $M(TeP^iPr_2NP^iPr_2Se)_2$ (**7**, M = Sn; **8**, M = Pb), were synthesized in 64−89% yields by metathesis of alkali-metal salts of the ligands with group 14 metal dihalides. Crystallographic characterization of the complexes revealed that **5**, **6**, and **8** engage in metal···chalcogen secondary bonds to generate dimers, whereas **7** is monomeric in the solid state. Multinuclear (^1H, ^{31}P, ^{77}Se, and ^{125}Te) solution NMR data for these homoleptic complexes evinced dynamic behavior leading to the equivalence of the two ligand environments. The Pb^{II} complex **6** was utilized as a single-source precursor to micrometer-scale lead telluride particles via two divergent techniques: aerosol-assisted chemical vapor deposition of the complex in THF/CH_2Cl_2 solution onto glass substrates yielded rectangular prisms, while solution injection of **6** in tri-*n*-octylphosphine onto $Si/SiO_2(100)$ substrates heated to 200−220 °C resulted in the formation of wires. PXRD and EDX analysis of the products confirmed the phase purity of the PbTe materials.

Introduction

The chemistry of the heavy p-block elements is often unique compared to that of the lighter elements, due to variation of properties including decreasing electronegativity and increasing metallic character and atomic radius as one descends a particular group of the periodic table. Additionally, relativistic effects often become significant for elements in the sixth period, such as thallium and lead. These effects, along with lower bond strengths when compared with lighter congeners, are responsible for the greater stability of lower oxidation states (Pb^{II} and Tl^{I}) for such elements. The large size of the heavy p-block elements combined with the possibility of stereochemical influence from a lone pair of electrons allows for several feasible coordination geometries, and hence the structural chemistry of these elements is worthy of investigation.

We are interested in the chemistry of dichalcogenido imidodiphosphinate ligands, $[(EPR_2)_2N]^-$ (E = O, S, Se, Te; R = alkyl, aryl), which possess two ligating chalcogen centers bridged by a P−N−P framework. There are several known Sn^{II} and Pb^{II} complexes of dichalcogenido imidodiphosphinate ligands (Table 1). Their solid-state structures demonstrate a variety of coordination geometries, indicating a stereochemical influence from the metal-centered lone pair. The complex $Pb(SPPh_2NPPh_2O)_2$ is dimeric through intermolecular lead···sulfur interactions, but the other examples are monomeric in nature. Given the lack of group 14 complexes containing tellurium-based ligands, such compounds were identified as targets for structural study. The soft, polarizable nature of tellurium centers within the $[(TeP^iPr_2)_2N]^-$ ligand, coupled with similarly soft tin and lead centers, affords the possibility of intermolecular interactions in such complexes in the solid state. Thus, the

Table 1. Tin(II) and Lead(II) Complexes of Some $[(EPR_2)_2N]^-$ Ligands

complex	molecular association	geometry at metal	ref
$Sn[(SePPh_2)_2N]_2$ (yellow)	monomeric	square-planar	1,2
$Sn[(SePPh_2)_2N]_2$ (red)	monomeric	tetragonal pyramidal	1,2
$Sn[(SeP^iPr_2)_2N]_2$	monomeric	square-planar	3
$Pb[(SePPh_2)_2N]_2$	monomeric	tetragonal pyramidal	2
$Pb[(SPPh_2)_2N]_2$	monomeric	ψ-octahedral	4
$Pb(SPPh_2NPPh_2O)_2$	dimeric	ψ-tbp	5

*To whom correspondence should be addressed. E-mail: chivers@ucalgary.ca. Fax: 1 403 289 9488. Tel: 1 403 220 5741.

(1) Cea-Olivares, R.; Novosad, J.; Woollins, J. D.; Slawin, A. M. Z.; García-Montalvo, V.; Espinosa-Pérez, G.; García, P. G. Y. *Chem. Commun.* **1996**, 519.
(2) García-Montalvo, V.; Novosad, J.; Kilian, P.; Woollins, J. D.; Slawin, A. M. Z.; García, P. G. Y.; López-Cardoso, M.; Espinosa-Pérez, G.; Cea-Olivares, R. *J. Chem. Soc., Dalton Trans.* **1997**, 1025.
(3) Cea-Olivares, R.; Moya-Cabrera, M.; García-Montalvo, V.; Castro-Blanco, R.; Toscano, R. A.; Hernández-Ortega, S. *Dalton Trans.* **2005**, 1017.
(4) Casas, J. S.; Castiñeiras, A.; Haiduc, I.; Sánchez, A.; Sordo, J.; Vásquez-López, E. M. *Polyhedron* **1994**, *13*, 2873.
(5) García-Montalvo, V.; Cea-Olivares, R.; Espinosa-Pérez, G. *Polyhedron* **1996**, *15*, 829.

 Published on Web 12/30/2009

preparation of these compounds was undertaken in order to examine their crystal structures and compare them with the known complexes listed in Table 1. A further incentive for this study was the possibility that such complexes could be used as single-source precursors (SSPs) to metal telluride semiconducting thin films.

Metal chalcogenides incorporating main-group metals such as PbS and $CuInSe_2$ are used as detection elements in infrared sensors and as photovoltaic materials in solar cells, respectively. The groups of O'Brien and Jain have developed various SSPs to these types of materials and utilized them for the deposition of thin films of the heavy p-block chalcogenides PbE,[6] In_2E_3,[7,8] and Bi_2E_3[9] (E = S, Se). Due to these advances, coupled with the increasing interest in tellurium-containing materials, coordination complexes of analogous Te-centered ligands are currently being investigated as SSPs to metal telluride solid-state materials.[10] We have previously reported the deposition of thin films of CdTe,[10b] In_2Te_3,[10c] and Sb_2Te_3[10d] using homoleptic complexes of the ditellurido imidodiphosphinate ligand $[(TeP^iPr_2)_2N]^-$.

The search for thermoelectric materials with a high figure of merit (*ZT*) has stimulated research into the preparation of low-dimensionality materials, which may show increased performance over their bulk counterparts. Lead telluride, a narrow band gap semiconductor with a large exciton Bohr radius, has received considerable attention in recent years, particularly with respect to the synthesis of nanoparticles with controlled shape and/or assembly by solvothermal techniques. Nanodimensional hollow boxes[11] and spheres[12] and flowers[13] of PbTe have been prepared in this way. Yang and co-workers have assembled PbTe nanocrystals with cubic, cuboctahedral, or octahedral morphologies with a dependence on the surfactant used and the ratio of Pb to Te in the solvothermal reaction mixture.[14] Urban and Murray have prepared monodisperse PbTe nanocrystals and shown that either glassy films or superlattices are formed when the particles are evaporatively deposited onto substrates, with a dependence on the solvent.[15]

The vast majority of methods for the preparation of PbTe nanoparticles require separate sources of Pb and Te: e.g., $Pb(OAc)_2$ and TeO_2. Arnold and Seligson have prepared the only previous example of a SSP to lead telluride, $[Pb(TeSi(SiMe_3)_3)_2]$.[16] Pyrolysis of this complex in a quartz tube led to the formation of PbTe powder contaminated by hydrocarbons (0.52 C and 0.14 H wt %). There is only one report of the use of vapor deposition to generate PbTe.[17] In that study, a PbTe/Au mixture was heated to >940 °C, and the nanoparticulate product was contaminated with elemental tellurium.

In this contribution, a series of Sn^{II} and Pb^{II} complexes of both ditellurido and heterodichalcogenido (Se/Te) imidodiphosphinate ligands has been prepared and structurally characterized. Their unique solid-state structures are discussed and compared to known complexes of ligands based on the lighter chalcogens (see Table 1). The utility of the lead(II) complex $Pb[(TeP^iPr_2)_2N]_2$ (**6**) as a SSP for PbTe is explored, and the deposition of phase-pure PbTe particles by two contrasting methods is discussed.

Experimental Section

Reagents and General Procedures. All solvents were dried and distilled from Na/benzophenone (except MeCN and CH_2Cl_2, which were dried and distilled from CaH_2) and stored over 4 Å molecular sieves prior to use. Deuterated solvents for NMR studies were degassed using at least three freeze−pump−thaw cycles and stored over 4 Å molecular sieves prior to use. The reagents $(Me_3Si)_2NH$ (97%), $^iPr_2PCl$ (96%), ^nBuLi (2.5 M in hexanes), NaH (99%), and Se (100 mesh, 99.5%) and Te powders (200 mesh, 99.8%) were purchased from Aldrich and used as received. The reagent TMEDA (99%, Aldrich) was stored over 4 Å molecular sieves prior to use. Lead(II) iodide was prepared by the aqueous reaction of lead(II) nitrate with potassium iodide; the product was dried by successive washing with MeOH and Et_2O and then heating under vacuum. Solutions of $(TMEDA)Li(TeP^iPr_2NP^iPr_2Se)$ in THF were prepared according to the literature procedure.[18] All manipulations were performed under an inert atmosphere of argon using standard glovebox and Schlenk techniques. Melting points (uncorrected) were obtained from samples sealed in capillary tubes under argon.

Instrumentation. ^1H, $^{31}P\{^1H\}$, $^{77}Se\{^1H\}$, and $^{125}Te\{^1H\}$ NMR spectra were recorded on either a Bruker DRX-400 or AMX-300 NMR spectrometer. Chemical shifts are reported in parts per million (ppm), relative to the external standards Me_4Si (^1H), 85% H_3PO_4 (^{31}P), Se_2Ph_2 (^{77}Se), and Te_2Ph_2 (^{125}Te). Elemental analyses were performed by the Analytical Services Laboratory, Department of Chemistry, University of Calgary. Powder X-ray diffraction patterns were measured with a Bruker D8 Advance diffractometer using Cu Kα radiation. Films were carbon-coated using an Edwards E306A coating system before SEM analyses were performed with a Philips XL30 FEG-SEM system. TEM analyses were carried out on a Philips CM200 200 kV TEM instrument. The sample was briefly sonicated in ethanol, which suspended the material, and then a drop of the suspension was placed on a TEM grid and allowed to dry. Both SEM and TEM instruments were equipped with EDAX DX-4 EDS accessories for EDX analyses. XPS analyses were recorded on a Kratos Axis Ultra XP spectrometer.

Synthesis of $HN(P^iPr_2)_2$ (1).[19] The reagent $(Me_3Si)_2NH$ (10.0 mL, 48.0 mmol) was added via syringe to a stirred solution of $^iPr_2PCl$ (14.636 g, 95.9 mmol) in toluene. The mixture was heated to 55 °C for 24 h, and then the volatiles were removed under vacuum. Hexane (75 mL) was added to the resulting oil,

(6) (a) Afzaal, M.; Ellwood, K.; Pickett, N. L.; O'Brien, P.; Raftery, J.; Waters, J. *J. Mater. Chem.* **2004**, *14*, 1310. (b) Kedarnath, G.; Kumbhare, L. B.; Dey, S.; Wadawale, A. P.; Jain, V. K.; Dey, G. K. *Polyhedron* **2009**, *28*, 2749.
(7) Afzaal, M.; Crouch, D.; O'Brien, P. *Mater. Sci. Eng., B* **2005**, *116*, 391.
(8) Afzaal, M.; Malik, M. A.; O'Brien, P. *Chem. Commun.* **2004**, 334.
(9) (a) Waters, J.; Crouch, D.; Raftery, J.; O'Brien, P. *Chem. Mater.* **2004**, *16*, 3289. (b) Chaudhari, K. R; Wadawale, A. P.; Ghoshal, S.; Chopade, S. M.; Sagoria, V. S.; Jain, V. K. *Inorg. Chim. Acta* **2009**, *362*, 1819.
(10) (a) For a review, see: Ritch, J. S.; Chivers, T.; Afzaal, M.; O'Brien, P. *Chem. Soc. Rev.* **2007**, *36*, 1622. (b) Garje, S. S.; Ritch, J. S.; Afzaal, M.; O'Brien, P.; Chivers, T. *J. Mater. Chem.* **2006**, *16*, 966. (c) Garje, S. S.; Copsey, M. C.; Afzaal, M.; O'Brien, P.; Chivers, T. *J. Mater. Chem.* **2006**, *16*, 4542. (d) Garje, S. S.; Eisler, D. J.; Ritch, J. S.; Afzaal, M.; O'Brien, P.; Chivers, T. *J. Am. Chem. Soc.* **2006**, *128*, 3120. (e) Kedarnath, G.; Jain, V. K.; Wadawale, A.; Dey, G. K. *Dalton Trans.* **2009**, 8378.
(11) Wang, W.; Poudel, B.; Wang, D.; Ren, Z. F. *Adv. Mater.* **2005**, *17*, 2110.
(12) Zou, G.; Liu, Z.; Wang, D.; Jiang, C.; Qian, Y. *Eur. J. Inorg. Chem.* **2004**, 4521.
(13) Zhang, G.; Lu, X.; Wang, W.; Li, X. *Chem. Mater.* **2007**, *19*, 5207.
(14) Mokari, T.; Zhang, M.; Yang, P. *J. Am. Chem. Soc.* **2007**, *129*, 9864.
(15) Urban, J. J.; Talapin, D. V.; Shevchenko, E. V.; Murray, C. B. *J. Am. Chem. Soc.* **2006**, *128*, 3248.
(16) Seligson, A. L.; Arnold, J. *J. Am. Chem. Soc.* **1993**, *115*, 8214.
(17) Zhang, B.; He, J.; Tritt, T. M. *Appl. Phys. Lett.* **2006**, *88*, 043119.
(18) Robertson, S. D.; Chivers, T. *Dalton Trans.* **2008**, 1765.
(19) The compound $HN(P^iPr_2)_2$ has been isolated using alternate routes such as (a) self-condensation of $H_2NP^iPr_2$ and (b) reaction of $LiHNP^iPr_2$ with $^iPr_2PCl$. In both cases ^{31}P but not ^1H NMR data were reported: (a) Ross, B.; Reetz, K.-P. *Chem. Ber.* **1979**, *112*, 1756. (b) Foss, V. L.; Veits, Y. A.; Chernykh, T. E.; Lutsenko, I. F. *J. Gen. Chem.* **1984**, *54*, 2386.

yielding a cloudy white solution. Filtration through a 0.45 μm pore size filter disk produced a colorless solution; removal of the volatiles under vacuum afforded a colorless oil. Successive dissolution of the oil in hexanes (3 × 20 mL) and solvent removal under vacuum afforded sticky white crystalline **1** (8.858 g, 74%). ^{1}H NMR (d_8-THF): δ 1.99 (br t, 1H, N*H*), 1.53 (sept, $^3J_{H-H}$ = 7 Hz, 4H, C*H*(CH_3)$_2$), 1.15−0.92 (m, 24H, CH(C*H*$_3$)$_2$). ^{31}P{^{1}H} NMR (d_8-THF): δ 69.4 (s). Some minor impurities are visible in the ^{1}H NMR spectrum of the product; it can be purified by sublimation[19a] or distillation[19b] but is sufficiently pure to use in the subsequent syntheses presented in this work.

Synthesis of NaN(P^{i}Pr$_2$)$_2$ (2). Method A. Hexane (5 mL) was layered on top of the reagent ^{n}BuNa (1.417 g, 17.7 mmol). After the mixture was cooled to −78 °C, THF (20 mL) precooled to −78 °C was added, and complete dissolution of the solid was attained with stirring for several minutes. The resulting clear, colorless solution was added dropwise via cannula to a solution of HN(P^{i}Pr$_2$)$_2$ (4.001 g, 16.0 mmol) in THF (25 mL) at −78 °C. After it was stirred for 2 h, the mixture was warmed to room temperature and the volatiles were removed under vacuum. The crude white product was suspended in hexanes, collected on a glass frit, washed with hexanes (3 × 20 mL), and dried under vacuum to afford **2** as a white powder (3.524 g, 81%). ^{1}H NMR (d_8-THF): δ 1.39 (sept, $^3J_{H-H}$ = 7 Hz, 4H, C*H*(CH_3)$_2$), 1.06−0.91 (m, 24H, CH(C*H*$_3$)$_2$). ^{31}P{^{1}H} NMR (d_8-THF): δ 87.4 (s).

Method B. Toluene (75 mL) was added to a mixture of solid HN(P^{i}Pr$_2$)$_2$ (8.769 g, 35.2 mmol) and NaH (855 mg, 35.6 mmol). The amine TMEDA (10.6 mL, 70.6 mmol) was added to the suspension, which was heated to 100 °C for 6 days. The resulting suspension was allowed to settle, and the yellow mother liquor was decanted. The crude solid was suspended in hexane, collected on a glass frit, washed with hexanes (3 × 20 mL), and dried under vacuum to afford **2** as a white powder (7.017 mg, 74%).

Synthesis of (TMEDA)Na[(TeP^{i}Pr$_2$)$_2$N] (3). Toluene (40 mL) was added to solid NaN(P^{i}Pr$_2$)$_2$ (3.503 g, 12.9 mmol) and Te powder (3.354 g, 26.3 mmol). The reagent TMEDA (1.94 mL, 12.9 mmol) was added to the suspension, which was heated to 80 °C for 2 h. The resulting mixture was filtered through a 0.45 μm pore size filter disk to give a clear yellow solution. Removal of the volatiles under vacuum afforded a yellow oil which slowly crystallized upon standing. Washing the oily product with hexane (3 × 20 mL) and drying under vacuum yielded **3** as a yellow polycrystalline powder (6.051 g, 73%). ^{1}H NMR (d_8-THF): δ 2.30 (s, 4H, (CH_3)$_2$N(C*H*$_2$)$_2$N(CH_3)$_2$), 2.16 (s, 12H, (C*H*$_3$)$_2$N(CH_2)$_2$N(C*H*$_3$)$_2$), 1.82−1.66 (m, 4H, C*H*(CH_3)$_2$), 1.19−1.01 (m, 24H, CH(C*H*$_3$)$_2$). ^{31}P{^{1}H} NMR (d_8-THF): δ 24.1 (s, $^1J_{Te-P}$ = 1487 Hz). ^{125}Te{^{1}H} NMR (d_8-THF): δ −754.3 (d, $^1J_{Te-P}$ = 1493 Hz). Anal. Calcd for $C_{18}H_{44}N_3Na_1P_2Te_2$: C, 33.64; H, 6.90; N, 6.54. Found: C, 33.12; H, 7.28; N, 6.18.

Synthesis of Pb[(SeP^{i}Pr$_2$)$_2$N]$_2$ (4). Et$_2$O (25 mL) was added to a mixture of solid (TMEDA)Na[(SeP^{i}Pr$_2$)$_2$N] (535 mg, 0.981 mmol) and PbI_2 (226 mg, 0.490 mmol). The resulting yellow suspension was stirred for 30 min, and then the volatiles were removed under vacuum to afford a white yellow oil. This oil was extracted with CH_2Cl_2 (30 mL) and filtered through Celite over a 0.45 μm pore size filter disk, and the volatiles were removed under vacuum to give a yellow oil. Washing with Et$_2$O (20 mL) yielded crystalline yellow **4** (263 mg, 53%). The NMR data matched those reported in the literature.[6] X-ray-quality crystals were obtained from a layered solution of the complex in CD_2Cl_2/hexanes at −30 °C.

Synthesis of Sn[(TeP^{i}Pr$_2$)$_2$N]$_2$ (5). THF (30 mL) was added to a mixture of solid (TMEDA)Na[(TeP^{i}Pr$_2$)$_2$N] (499 mg, 0.776 mmol) and $SnCl_2$ (76 mg, 0.40 mmol). The resulting orange solution was stirred at room temperature for 30 min before the volatiles were removed under vacuum. Upon extraction with toluene (20 mL), filtration through a 0.45 μm pore size filter disk, and removal of the volatiles under vacuum, dark orange solid **5** was obtained (388 mg, 89%). ^{1}H NMR (d_8-THF, 298 K): δ 2.18−2.03 (m, 8 H, −C*H*(CH_3)$_2$), 1.30−1.04 (m, 48 H, −CH(C*H*$_3$)$_2$). ^{31}P{^{1}H} NMR (d_8-THF, 253 K): δ 35.2 (s, $^2J_{P-P}$ = 26 Hz, $^2J_{Sn-P}$ = 40 Hz, $^1J_{Te-P}$ = 1346 Hz). ^{125}Te{^{1}H} NMR (d_8-THF, 243 K): δ −497.4 (d, $^1J_{Te-P}$ = 1347 Hz). Anal. Calcd for $C_{24}H_{56}N_2P_4SnTe_4$: C, 25.61; H, 5.01; N, 2.49. Found: C, 25.50; H, 4.99; N, 2.32. X-ray-quality crystals were obtained from a solution of the complex in THF at −30 °C.

Synthesis of Pb[(TeP^{i}Pr$_2$)$_2$N]$_2$ (6). Et$_2$O (30 mL) at 0 °C was added to a mixture of solid (TMEDA)Na[(TeP^{i}Pr$_2$)$_2$N] (1.256 g, 2.0 mmol) and PbI_2 (450 mg, 1.0 mmol). The resulting cloudy orange solution was stirred at 0 °C for 30 min and then allowed to settle. The pale yellow-orange solution was decanted, and the remaining orange solid was extracted with CH_2Cl_2 (30 mL). After some of the solid NaI was allowed to settle, the solution was filtered through a 0.45 μm pore size filter disk to afford a clear orange solution. Removal of the volatiles under vacuum yielded a crystalline orange solid, which was washed with 0 °C Et$_2$O (3 × 15 mL) and dried under vacuum to give pure **6** (760 mg, 64%; mp 138 °C dec). ^{1}H NMR (CD_2Cl_2): δ 2.04−2.17 (m, 8 H, C*H*(CH_3)$_2$), 1.38−1.17 (m, 48 H, CH(C*H*$_3$)$_2$). ^{31}P{^{1}H} NMR (CD_2Cl_2): δ 32.7 (s, $^1J_{Te-P}$ = 1318 Hz). ^{125}Te{^{1}H} NMR (CD_2Cl_2): δ −547.3 (d, $^1J_{Te-P}$ = 1323 Hz). Anal. Calcd for $C_{24}H_{56}N_2P_4PbTe_4$: C, 23.71; H, 4.65; N, 2.31. Found: C, 23.58; H, 4.75; N, 2.40. X-ray-quality crystals were obtained from a layered solution of the complex in CH_2Cl_2/hexanes at 5 °C.

Synthesis of Sn(TeP^{i}Pr$_2$NP^{i}Pr$_2$Se)$_2$ (7). A cold (−78 °C) solution of (TMEDA)Li(TeP^{i}Pr$_2$NP^{i}Pr$_2$Se) (0.970 mmol) in THF (40 mL) was prepared according to the literature method.[18] This was added to a cold (−78 °C) solution of $SnCl_2$ (92 mg, 0.485 mmol) in THF (20 mL), and the resulting yellow solution was stirred at −78 °C for 30 min and then at room temperature for 30 min. The volatiles were removed under vacuum, and the resulting oil was extracted with CH_2Cl_2 (25 mL), filtered through Celite over a 0.45 μm pore size filter disk, and pumped under vacuum to give a yellow oil. This was washed with hexamethyldisiloxane (HMDSO, 3 × 10 mL) to afford yellow crystalline **7** (337 mg, 68%). ^{1}H NMR (CD_2Cl_2): δ 2.26−2.12 (m, 4 H, −C*H*(CH_3)$_2$), 2.12−1.99 (m, 4 H, −C*H*(CH_3)$_2$), 1.32−1.10 (m, 48 H, −CH(C*H*$_3$)$_2$). ^{31}P{^{1}H} NMR (CD_2Cl_2): δ 63.7 (d, $^2J_{P-P}$ = 28 Hz, $^2J_{Sn-P}$ = 79 Hz, $^1J_{Se-P}$ = 575 Hz, *P*−Se), 34.6 (d, $^2J_{P-P}$ = 28 Hz, $^2J_{Sn-P}$ = 38 Hz, $^1J_{Te-P}$ = 1247 Hz, *P*−Te). ^{77}Se{^{1}H} NMR (CD_2Cl_2): δ −185.8 (d of d, $^1J_{Se-P}$ = 575 Hz, $^3J_{Se-P}$ = 14 Hz, $^1J_{Se-Sn}$ = 440 Hz). ^{125}Te{^{1}H} NMR (CD_2Cl_2): δ −454.2 (d, $^1J_{Te-P}$ = 1242 Hz, $^1J_{Te-Sn}$ = 748 Hz). Anal. Calcd for $C_{24}H_{56}N_2P_4Se_2SnTe_2$: C, 28.03; H, 5.49; N, 2.72. Found: C, 28.20; H, 5.33; N, 2.73. X-ray-quality crystals were obtained from a concentrated solution of the complex in Et$_2$O at 5 °C.

Synthesis of Pb(TeP^{i}Pr$_2$NP^{i}Pr$_2$Se)$_2$ (8). The lead(II) complex **8** was prepared by a procedure similar to that for **7**, with PbI_2 (212 mg, 0.460 mmol) reacting with (TMEDA)Li(TeP^{i}Pr$_2$NP^{i}Pr$_2$Se) (0.914 mmol) to produce an orange powder (398 mg, 78%). ^{1}H NMR (CD_2Cl_2): δ 2.38−2.17 (m, 4 H, −C*H*(CH_3)$_2$), 2.17−2.05 (m, 4 H, −C*H*(CH_3)$_2$), 1.32−1.13 (m, 48 H, −CH(C*H*$_3$)$_2$). ^{31}P{^{1}H} NMR (CD_2Cl_2): δ 61.1 (d, $^2J_{P-P}$ = 29 Hz, $^1J_{Se-P}$ = 574 Hz), 29.7 (d, $^2J_{P-P}$ = 29 Hz, $^1J_{Te-P}$ = 1235 Hz). ^{77}Se{^{1}H} NMR (CD_2Cl_2): δ −230.1 (d, $^1J_{Se-P}$ = 574 Hz). ^{125}Te{^{1}H} NMR (CD_2Cl_2): δ −493.8 (d, $^1J_{Te-P}$ = 1253 Hz). Anal. Calcd for $C_{24}H_{56}N_2P_4PbSe_2Te_2$: C, 25.81; H, 5.05; N, 2.51. Found: C, 25.63; H, 5.08; N, 2.37. X-ray-quality crystals were obtained from a concentrated solution of the complex in Et$_2$O at 5 °C.

X-ray Crystallography. A suitable crystal of each complex was coated in Paratone 8277 oil (Exxon) and mounted on a glass fiber. Data were collected at 173 K on a Nonius KappaCCD diffractometer using Mo Kα radiation (λ = 0.710 73 Å) with ω and φ scans with the Nonius COLLECT program.[20] The unit

(20) *COLLECT, Data Collection Software*; Nonius BV, **1997**−**2001**.

Table 2. Crystallographic Data for **4**–**8**[a]

	4	**4**·$n$$CD_2Cl_2$	**5**	**6**	**7**	**8**
chem formula	$C_{24}H_{56}N_2P_4PbSe_4$	$C_{24}H_{56}N_2P_4PbSe_4$	$C_{24}H_{56}N_2P_4SnTe_4$	$C_{24}H_{56}N_2P_4PbTe_4$	$C_{24}H_{56}N_2P_4Se_2SnTe_2$	$C_{24}H_{56}N_2P_4PbSe_2Te_2$
formula wt	1019.62	1019.62	1125.68	1214.19	1028.40	1116.90
cryst syst	monoclinic	triclinic	monoclinic	monoclinic	monoclinic	monoclinic
space group	$C2/c$	$P\bar{1}$	$C2/c$	$C2/c$	$P2_1/c$	$C2/c$
a (Å)	32.019(6)	9.4939(19)	34.829(7)	34.833(7)	23.990(5)	34.625(7)
b (Å)	9.4607(19)	14.531(3)	9.792(2)	9.795(2)	10.029(2)	9.7284(19)
c (Å)	27.247(5)	15.967(3)	25.993(5)	26.044(5)	15.696(3)	25.834(5)
α (deg)	90	74.94(3)	90	90	90	90
β (deg)	117.14(3)	87.83(3)	120.00(3)	120.25(3)	90.20(3)	120.15(3)
γ (deg)	90	85.25(3)	90	90	90	90
V (Å^3)	7345(3)	2119.5(8)	7677(4)	7676(4)	3776.4(13)	7524(3)
Z	8	2	8	8	4	8
D_{calcd} (g cm^{-3})	1.844	1.598	1.948	2.101	1.809	1.972
μ(Mo Kα) (mm^{-1})	8.750	7.580	3.829	7.559	4.305	8.126
R_{int}	0.0314	0.0373	0.0499	0.0342	0.0377	0.0329
R1 ($I > 2\sigma(I)$)[b]	0.0306	0.0463	0.0385	0.0345	0.0429	0.0595
wR2 (all data)[c]	0.0744	0.1009	0.0920	0.0825	0.1070	0.1638
GOF on F^2	1.100	1.093	1.050	1.029	1.066	1.085

[a] λ(Mo Kα) = 0.710 73 Å, T = 173(2) K. [b] $R1 = \sum||F_o| - |F_c||/\sum|F_o|$. [c] $wR2 = [\sum w(F_o^2 - F_c^2)^2/\sum wF_o^4]^{1/2}$.

cell parameters were calculated and refined from the full data set. Crystal cell refinement and data reduction were carried out by using the Nonius DENZO package.[21] After reduction, the data were corrected for absorption based on equivalent reflections using SCALEPACK.[21] The structures were solved by direct methods with SHELXS-97,[22] and refinement was carried out on F^2 against all independent reflections by the full-matrix least-squares method by using the SHELXL-97 program.[23] Hydrogen atoms were calculated geometrically and were riding on their respective atoms. All non-hydrogen atoms were refined with anisotropic thermal parameters.

Crystallographic data are summarized in Table 2. No special considerations were necessary for compounds **4** (unsolvated), **5**, **6**, and **7**. For the complex **4**·$n$$CD_2Cl_2$, positional disorder was observed for one isopropyl group, which was modeled as a 60:40 isotropic mixture over two positions. A disordered CD_2Cl_2 molecule was present in the unit cell, but no suitable refinement model could be found. The electron density associated with this fragment was removed using SQUEEZE (PLATON),[24] leaving a void of ca. 384 Å^3. For complex **8**, positional disorder of the chalcogen atoms was observed at all four sites in the molecule. Each position was assigned one selenium and one tellurium center, and the values of d(P–E) (E = Se, Te) were restrained to be equal to the values found in the symmetric complexes **4** and **6**. The pairs of same chalcogen atoms for each ligand were further restrained to possess the same anisotropic displacement parameters. Under these conditions, approximate site occupancy factors of 64:36 and 70:30 were determined for the two ligand environments.

General Procedure for AACVD Experiments. Glass substrates for AACVD runs were cut from microscope slides. The substrates were soaked in concentrated nitric acid overnight, thoroughly rinsed with deionized water and then acetone, and dried in an oven prior to use. Substrates were handled using only forceps to avoid transfer of dust or oils to the surface. In a typical experiment, the AACVD apparatus was assembled inside a fume hood as previously described.[25] Prior to deposition, the tube furnace was heated to allow the substrates to reach the desired temperature, and argon gas flow was permitted for at least 15 min to purge the apparatus of oxygen and moisture. A solution of the SSP (typically 100 mg of precursor in 10 mL of solvent) was prepared using dry, degassed solvent and then transferred to the three-neck flask via glass syringe through the septum of the free side neck. Deposition experiments began upon starting the humidifier and continued until most of the solution had been vaporized and passed through the reactor tube. After 1–2 h, the humidifier and tube furnace were shut off. The substrates were cooled to room temperature under the flow of argon before handling to minimize oxidation.

General Procedure for Solution Injection Experiments. Si/SiO_2(100) wafers were cleaned with acetone, 2-propanol, and deionized water. A degassed suspension of the complex **6** (0.082 mM) in tri-n-octylphosphine (TOP) was prepared and injected onto 0.5 cm^2 Si/SiO_2(100) substrates. The substrates were preheated to 220 °C under N_2. After 20 min, the substrates were finally cooled to room temperature under N_2 before removal.

Results and Discussion

The bis(phosphino)amine $HN(P^iPr_2)_2$ (**1**) is prepared from the commercially available reagents $(Me_3Si)_2NH$ and $^iPr_2PCl$. This compound is often described in the literature as an in situ reagent,[26] but information on its isolation and characterization is limited.[19] The sodiation of **1**, which is accomplished using either NaH or ^{n}BuNa, yields the sodium amide $NaN(P^iPr_2)_2$ (**2**), which has been previously reported without detailed characterization.[18,27] Oxidation of **2** with elemental tellurium in the presence of *N,N,N′,N′*-tetramethylethylenediamine (TMEDA) yields the ditellurido ligand (TMEDA)Na[$(TeP^iPr_2)_2N$] (**3**; Scheme 1).[28]

Synthesis of (TMEDA)Na[$(TeP^iPr_2)_2N$] and the Complexes M[$(EP^iPr_2)_2N]_2$ (4, M = Pb, E = Se; 5, M = Sn, E = Te; 6, M = Pb, E = Te). The lead(II) complex $Pb[(SePPh_2)_2N]_2$ has been crystallographically characterized; however, the isopropyl analogue $Pb[(SeP^iPr_2)_2N]_2$ (**4**)

(21) Otwinowski, Z.; Minor, W. In *Methods in Enzymology*; Carter, C. W., Sweet, R. M., Eds.; Academic Press: New York, 1997; Vol. *276*, pp 307–326.
(22) Sheldrick, G. M. *SHELXS-97, Program for Solution of Crystal Structures*; University of Göttingen, Göttingen, Germany, **1997**.
(23) Sheldrick, G. M. *SHELXL-97, Program for Refinement of Crystal Structures*; University of Göttingen, Göttingen, Germany, **1997**.
(24) Van Sluis, P.; Spek, A. L. *Acta Crystallogr., Sect. A* **1990**, *46*, 194.
(25) Park, J.-H.; Afzaal, M.; Kemmler, M.; O'Brien, P.; Otway, D. J.; Raftery, J.; Waters, J. *J. Mater. Chem.* **2003**, *13*, 1942.
(26) Cupertino, D.; Birdsall, D. J.; Slawin, A. M. Z.; Woollins, J. D. *Inorg. Chim. Acta* **1999**, *290*, 1.
(27) Ritch, J. S.; Chivers, T.; Eisler, D. J.; Tuononen, H. M. *Chem. Eur. J.* **2007**, *13*, 4643.
(28) Although **3** has been previously reported, full details of the synthesis and NMR characterization were not disclosed: Chivers, T.; Eisler, D. J.; Ritch, J. S. *Dalton Trans.* **2005**, 2675.

Scheme 1

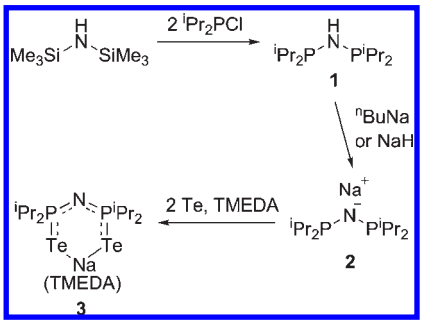

was previously identified only by NMR spectroscopy.[6] Therefore, this complex was prepared and crystallized in order to compare its solid-state structure with those of tellurium-based complexes. The reported synthesis of **4** involves in situ deprotonation of $HN(SeP^iPr_2)_2$ with NaOMe in MeOH, followed by metathesis with $PbCl_2$. For this study, an alternative route using the convenient sodium salt $(TMEDA)Na[(SeP^iPr_2)_2N]$[27] was used (eq 1), giving a yellow product in 53% yield.

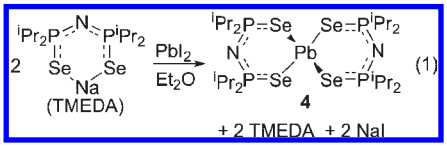

The corresponding tellurium-containing Sn^{II} complex $Sn[(TeP^iPr_2)_2N]_2$ (**5**) was obtained in 89% yield as an air- and moisture-sensitive orange powder by the reaction of $(TMEDA)Na[(TeP^iPr_2)_2N]$ with $SnCl_2$ in Et_2O. Similarly, reaction of the same reagent with PbI_2 in Et_2O yielded the air- and moisture-sensitive orange solid $Pb[(TeP^iPr_2)_2N]_2$ (**6**) in 64% yield (eq 2). The tin(II) complex **5** was soluble in common organic solvents, but the solubility of **6** was low in solvents such as toluene and THF. However, CH_2Cl_2 and MeCN were found to be suitable solvents for this lead(II) complex. X-ray-quality crystals of **4**–**6** were obtained from CD_2Cl_2/hexanes, THF, and CH_2Cl_2/hexanes, respectively. A thermal ellipsoid plot of **6** is given in Figure 1 as representative of the three isostructural complexes; selected bond lengths and bond angles are displayed in Table 3.

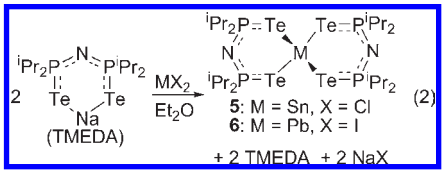

Both the selenium- and tellurium-based complexes were found to be associated in the solid state via M···E interactions with adjacent molecules to give C_2-symmetric dimers. Taking these interactions into account, the geometry at the metal centers is best described as distorted square pyramidal. The metal-based lone pair of electrons is thus occupying the vacant octahedral coordination site. The M–Te bond lengths vary significantly within each formula unit (**5**, 2.883(1)–3.150(1) Å; **6**, 2.946(1)–3.308(1) Å), with the apical distance being shortest in both cases. The bond lengths in the basal plane are significantly longer, most noticeably for the Te center involved in the intermolecular interaction, which itself is

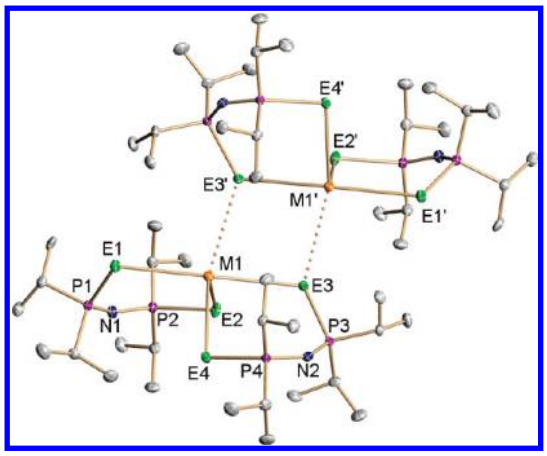

Figure 1. Thermal ellipsoid plot (30% probability) of **6** as representative of complexes **4** (M = Pb, E = Se), **5** (M = Sn, E = Te), and **6** (M = Pb, E = Te). The prime symbol denotes atoms generated by a crystallographic inversion center: $-x, y, {}^1/_2 - z$.

Table 3. Selected Bond Lengths (Å) and Bond Angles (deg) for **4**–**6**[a]

	4 (M = Pb, E = Se)	**5** (M = Sn, E = Te)	**6** (M = Pb, E = Te)
M(1)–E(1)	2.991(1)	3.150(1)	3.196(1)
M(1)–E(2)	2.777(1)	2.883(1)	2.946(1)
M(1)–E(3)	3.099(1)	3.230(1)	3.308(1)
M(1)–E(4)	2.875(1)	2.985(1)	3.084(1)
M(1)···E(3′)	3.574(2)	3.707(1)	3.597(1)
E(1)–P(1)	2.168(1)	2.410(2)	2.411(1)
P(1)–N(1)	1.584(4)	1.589(6)	1.580(4)
N(1)–P(2)	1.578(4)	1.573(6)	1.587(4)
P(2)–E(2)	2.202(1)	2.461(2)	2.452(1)
E(3)–P(3)	2.179(1)	2.426(2)	2.428(1)
P(3)–N(2)	1.590(4)	1.598(6)	1.599(4)
N(2)–P(4)	1.591(3)	1.586(6)	1.587(4)
P(4)–E(4)	2.190(1)	2.439(2)	2.430(1)
P(1)–N(1)–P(2)	147.4(3)	147.3(4)	148.2(3)
P(3)–N(2)–P(4)	140.7(2)	141.8(4)	142.6(3)
E(1)–M(1)–E(3)	173.61(1)	169.48(2)	169.54(3)
E(2)–M(1)–E(4)	96.68(2)	93.25(2)	93.22(2)
E(4)–M(1)–E(3′)	159.87(1)	162.27(2)	161.81(1)
E(2)–M(1)–E(3′)	99.07(2)	96.58(2)	96.04(2)

[a] Symmetry operation (prime symbol): $-x, y, {}^1/_2 - z$.

within the sums of the van der Waals radii for the elements (d(Sn···Te) = 3.707(1) Å, $\sum_{vdW}$ = 4.23 Å; d(Pb···Te) = 3.597(1) Å, $\sum_{vdW}$ = 4.08 Å). Interestingly, the intermolecular distance is shorter in the case of lead(II) by ca. 0.1 Å, which may indicate a stronger interaction in this case. An alternative explanation is that the lone pair of electrons is closer to the lead center due to relativistic contraction of the orbital. The P–N distances observed in **5** and **6** are all equal within experimental errors (1.573(6)–1.599(4) Å), while the P–Te bond lengths vary more significantly (**5**, 2.410(2)–2.461(2) Å; **6**, 2.411(1)–2.452(1) Å). For the latter, the longest distances were seen for the apically bound Te center.

The selenium-based complex $Pb[(SeP^iPr_2)_2N]_2$ (**4**) was structurally very similar to the complexes **5** and **6**, featuring a square-pyramidal geometry at the lead center and with Pb–Se bond lengths comparable to those of the phenyl-substituted analogue $Pb[(SePPh_2)_2N]_2$ (R = ^{i}Pr, 2.777(1)–3.099(1) Å; R = Ph, 2.874(3)–2.997(2) Å).[2] The Pb···Se secondary bonding distance was found to be 3.574(2) Å. Interestingly, when **4** was grown from a

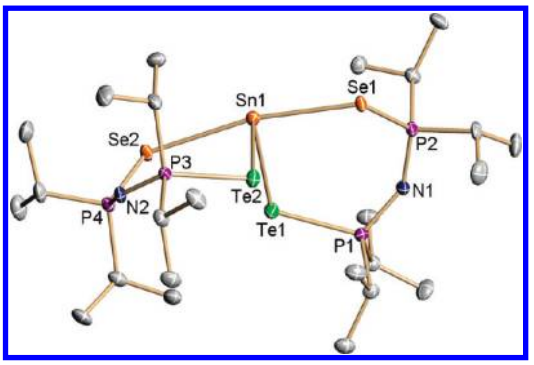

Figure 2. Thermal ellipsoid plot (30% probability) of **7**.

different solvent system (CD_2Cl_2/HMDSO), crystals with different unit cell parameters were obtained. The solid-state structure of these unique crystals was determined and also revealed a dimeric motif. There was a free molecule of disordered CD_2Cl_2 solvent in the lattice, and the geometry of the dimeric structure was somewhat different. Rather than a square-pyramidal arrangement, the metal centers are best described as distorted trigonal bipyramidal, as evidenced by the bond angles Se4−Pb1−Se3A and Se2−Pb1−Se3A (120.91(2) and 138.84(3)°, respectively, compared with 159.87(1) and 99.07(2)° in the other structural isomer). The intermolecular Pb···Se distance in this alternate crystal structure was found to be 3.709(1) Å, ca. 0.14 Å longer than that in the nonsolvated crystals.

The structural studies of the complexes **4**−**6** indicate that a dimeric structure is favored. In the case of the selenium-based Pb^{II} complex **4**, the isopropyl-substituted ligand seems to engender a dimeric structure, as the reported phenyl-substituted derivative was demonstrated to be a monomer in the solid state.[2]

Solution NMR data were collected for the Sn^{II} complex **5** in d_8-THF and for the less soluble Pb^{II} complex **6** in CD_2Cl_2. The $^{31}P\{^1H\}$ NMR spectra for the two complexes were similar, each exhibiting a singlet resonance indicative of a lone phosphorus environment. In view of the weak intermolecular interactions in **5** and **6** in the solid state, it is possible that dissociation into two monomers occurs in solution. Nevertheless, the observation of a single ^{31}P NMR resonance indicates that an exchange process renders the four unique P environments equivalent on the NMR time scale in solution. The ^{31}P nuclei for **5** and **6** resonated in the narrow range of δ 32.7−35.1, and both exhibited ^{125}Te satellites with $^1J_{Te-P}$ = 1323−1346 Hz. For **5**, $^{117/119}Sn$ satellites were observed in the $^{31}P\{^1H\}$ NMR spectrum, with values of 40 Hz. However, no coupling to ^{207}Pb was seen in complex **6**. Doublet resonances were observed in the $^{125}Te\{^1H\}$ NMR spectra of these compounds, with the chemical shift of the lead(II) complex **5** being more shielded than the tin(II) analogue **6** (δ −547.3 and −497.4, respectively).

Synthesis of $M(TeP^iPr_2NP^iPr_2Se)_2$ (7, M = Sn; 8, M = Pb). In order to probe whether or not Sn^{II} or Pb^{II} complexes of the mixed-donor ligand $[TeP^iPr_2NP^iPr_2Se]^-$ would dimerize selectively through either Pb···Se or Pb···Te interactions, these complexes were prepared and structurally characterized. The reactions of $SnCl_2$ or PbI_2 with the lithium derivative (TMEDA)Li-$(TeP^iPr_2NP^iPr_2Se)$[18] were carried out in THF, and the products $M(TeP^iPr_2NP^iPr_2Se)_2$ (**7**, M = Sn; **8**, M = Pb) were isolated as yellow powders in 68−78% yield (eq 3). Complex **8** was recrystallized from Et_2O to give X-ray-quality crystals. The structural analysis revealed a dimeric arrangement; however, the selenium and tellurium centers were disordered over all of the chalcogen sites. Restraints were used in the refinement of the crystal structure, and a detailed discussion of bond lengths or angles is therefore unjustified. Nonetheless, on the basis of the model used in the final solution (R1 = 5.95%), 64% of the dimerization interactions involve a Pb···Te contact, showing a definite preference for the heavier chalcogen center. The estimated Pb···Te distance is ca. 3.57 Å, similar to the value of 3.597(1) Å found in the all-tellurium complex **6**.

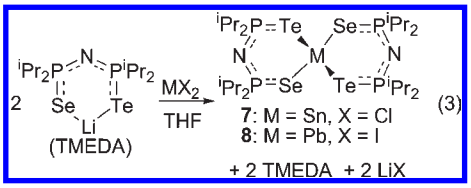

Suitable X-ray-quality crystals of the mixed-chalcogen Sn^{II} complex **7** were obtained from a concentrated solution in Et_2O. A thermal ellipsoid plot is shown in Figure 2, and selected bond lengths and bond angles are presented in Table 4. In contrast to **5** and **6**, the complex **7** is monomeric with no metal−chalcogen interactions within the van der Waals limits. Furthermore, unlike the case for the Pb^{II} complex **8**, there is no chalcogen disorder in **7**.

Table 4. Selected Bond Lengths (Å) and Bond Angles (deg) for **7**

Sn(1)−Te(1)	2.878(1)	N(1)−P(2)	1.584(5)
Sn(1)−Te(2)	2.891(1)	P(2)−Se(1)	2.215(2)
Sn(1)−Se(1)	2.986(1)	Te(2)−P(3)	2.439(2)
Sn(1)−Se(2)	3.023(1)	P(3)−N(2)	1.593(5)
Te(1)−P(1)	2.428(2)	N(2)−P(4)	1.594(5)
P(1)−N(1)	1.590(5)	P(4)−Se(2)	2.194(2)
P(1)−N(1)−P(2)	142.5(3)	Se(1)−Sn(1)−Se(2)	170.76(2)
P(3)−N(2)−P(4)	140.7(3)	Te(1)−Sn(1)−Te(2)	98.77(2)

The tin center possesses a distorted seesaw geometry, with the more electronegative selenium atoms occupying the axial positions and the tellurium centers lying along the equatorial plane. The vacant coordination site is indicative of a stereochemically active lone pair of electrons at the tin center. The Sn−Se bond lengths of 2.986(1)−3.023(1) Å are substantially longer than those found in the isopropyl-substituted square-planar complex $Sn[(SeP^iPr_2)_2N]_2$ (2.640(1)−2.660(1) Å)[3] but similar to the values seen in the analogous phenyl-substituted compound $Sn[(SePPh_2)_2N]_2$ (2.803(2)−2.943(2) Å).[1,2] The Sn−Te distances (2.878(1)−2.891(1) Å) were found to be shorter than the Sn−Se distances. This may be attributable to a repulsive influence of the Sn^{II} lone pair, which is closer to the selenium centers and elongates the Sn−Se bonds. The metrical parameters of the ligands were in accord with those seen in the complexes **5** and **6**. P−N distances were equal within the experimental errors, and the P−E (E = Se, Te) bond lengths were not significantly different from those found in similar complexes.

On the basis of the crystal structures obtained for complexes **5**−**8**, along with data for known complexes (see Table 1), the factors that determine the coordination

geometry of the metal, as well as the state of aggregation, seem to be subtle, low-energy interactions easily disrupted or influenced by crystal packing forces or small changes to the electronic properties of the ligand introduced by a change in the organic substituents on phosphorus. It is quite possible that different structural arrangements for these tellurium-containing complexes could be obtained by using different crystallization conditions. Dimeric solid-state structures have been demonstrated as favorable in most cases for complexes of tellurium-containing ligands, owing to the formation of weak M···Te associations.

The multinuclear NMR spectra of **7** and **8** were recorded in CD_2Cl_2 solutions. Two mutually coupled doublets were apparent for each complex in the $^{31}P\{^1H\}$ NMR spectra, resonating at δ 61.1−63.7 for the selenium-bound sites and δ 29.7−34.6 for the centers directly bound to tellurium, with appropriate chalcogen satellites associated with each resonance ($^1J_{Se-P}$ = 574 − 575 Hz; $^1J_{Te-P}$ = 1235 − 1247 Hz). In addition, $^2J_{Sn-P}$ satellites were seen on each resonance for complex **7** (79 and 38 Hz for the selenium- and tellurium-bound phosphorus sites, respectively). The $^{77}Se\{^1H\}$ and $^{125}Te\{^1H\}$ NMR spectra were also obtained for complexes **7** and **8**, and the chemical shifts indicate a shielding effect in each case on going from Sn to Pb ($\delta(^{77}Se)$ −185.8 (**7**) and −230.1 (**8**); $\delta(^{125}Te)$ −454.2 (**7**) and −493.8 (**8**)). Satellites due to $^{117/119}Sn$ were observed in these spectra for complex **7**, with values of $^1J_{Sn-Se}$ = 440 Hz and $^1J_{Te-Sn}$ = 748 Hz. Overall, the NMR spectra are consistent with solution structures of **7** and **8** which possess one unique site for each of the selenium- and tellurium-bound phosphorus centers on the NMR time scale. In the case of the monomeric complex **7** this is likely due to conformational flexibility, such as Berry pseudorotation,[29] in solution leading to an equivalence of crystallographically independent sites. While the state of aggregation for complex **8** in solution is unknown, it is possible that it too is monomeric, given the weak nature of the Pb···E contacts seen in this new group of complexes.

Synthesis of Lead Telluride using Complex 6. AACVD of the tin complex **5** was attempted with toluene solutions over the temperature range 375−475 °C; however, in all cases only hexagonal Te was obtained. Thermogravimetric analysis under N_2 showed that the Pb^{II} complex **6** decomposes in one step between 197 and 304 °C (Supporting Information). Our initial attempts to prepare thin films of PbTe involved the AACVD of $Pb[(TeP^iPr_2)_2N]_2$ (**6**) onto glass substrates. The solubility of the complex is low in common organic solvents such as THF and toluene; but it is better in CH_2Cl_2 and MeCN. Sufficient solubility of **6** was achieved in THF/CH_2Cl_2 (1:1), MeCN, and $MeCN/CH_2Cl_2$ (1:1). The AACVD of **6** using substrate temperatures below 475 °C gave films composed of PbTe and Te, as determined by PXRD. The as-deposited gray films were nonadherent and could be easily wiped off the surface, indicating that the lead telluride "films" were of poor quality. Experiments at 475 °C (Ar flow rate 160−240 sccm) gave aggregates of particles with poor coverage of the substrate surface, but the deposited materials were confirmed by PXRD to be phase-pure cubic PbTe. The best results came from using a THF/CH_2Cl_2 solution (calculated lattice constant a = 6.461 Å, comparable to the accepted value of 6.459 Å, ICDD No. 038-1435). An SEM image of the PbTe particles deposited under these conditions is shown in Figure 3. The formation of submicrometer-sized rectangular prisms is seen; the surface coverage is poor, with ca. half of the substrate surface remaining uncovered. This held true for the other solvent systems as well. Additionally, significant amounts of precursor always remained in the precursor solution flask at the end of the AACVD experiments, indicating poor delivery.

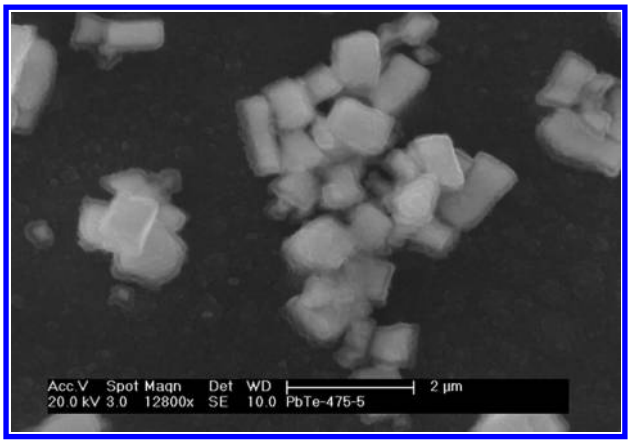

Figure 3. SEM micrograph of PbTe particles obtained from AACVD at 475 °C.

In view of the difficulties in obtaining good-quality films, as well as the low solubility of the precursor in most solvents, we sought an alternate route to prepare PbTe films. A hot-injection process was used to introduce the precursor onto a preheated substrate at specific temperature. A degassed suspension of the precursor (0.082 mM) in tri-*n*-octylphosphine (TOP) was directly injected onto a preheated $Si/SiO_2(100)$ substrate. The PXRD patterns showed the exclusive formation of cubic PbTe with calculated lattice constants of a = 6.456 Å (200 °C) and 6.455 Å (220 °C) (Figure 4a,b). At higher injection temperatures, the crystallinity of the films significantly improved, as indicated by the presence of sharper and narrower diffraction peaks. Furthermore, the PXRD on the films showed a significant preferred orientation possibility, reflecting interactions with the crystalline Si/SiO_2 substrate surface. The apparently homogeneous nature of the films was evident from SEM studies, which indicated PbTe wires without any directional order (Figure 4c). No rods corresponding to elemental tellurium were observed. The widths of wires vary between 0.2 and 1.1 μm, and their lengths ranges from tens of micrometers to several micrometers. It is important to realize that the surfaces of the substrates were not chemically functionalized, which might prompt the growth of wires. It is more likely that these wires are self-generated on the orientated Si/SiO_2 surfaces. Quantitative energy-dispersive X-ray (EDX) analysis obtained from several wires revealed a Pb:Te ratio of 1:1, respectively (within the errors of the method). EDX analysis at different axial positions of the wires showed no detectable change in composition. A HR-TEM image of the same film showed well-resolved lattice planes corresponding to (220) of cubic PbTe (calcd 0.226 nm,

(29) Berry, R. S. *J. Chem. Phys.* **1960**, *32*, 933.

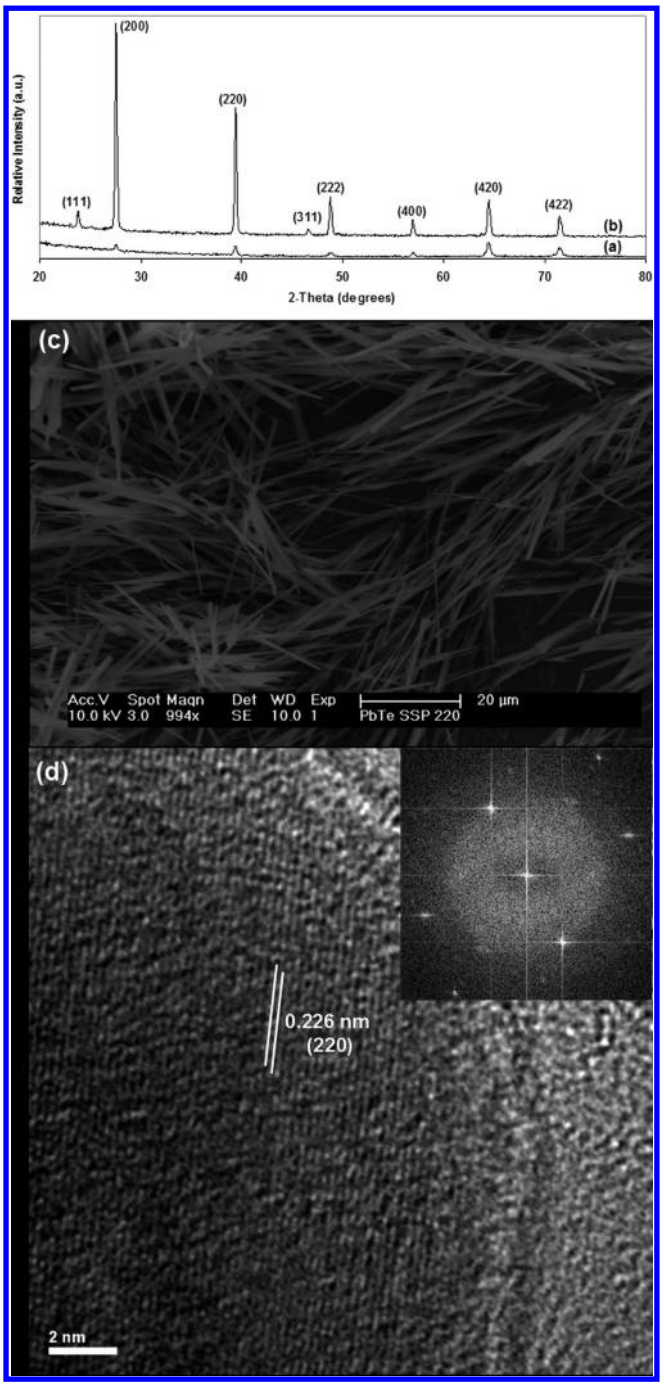

Figure 4. PXRD patterns of PbTe at (a) 200 °C and (b) 220 °C by the injection method and SEM (c) and HRTEM (d) of PbTe wires deposited at 220 °C (the inset shows the SAED pattern of one PbTe wire).

lit. 0.228 nm) (Figure 4d). The corresponding selected area electron diffraction (SAED) pattern also confirmed the single-crystal nature of the material (Figure 4d, inset).

The chemical composition of the wires was probed by X-ray photoelectron spectroscopy (XPS), which showed a highly oxidized surface with oxygen content of ~20 wt % (Supporting Information). PXRD of the films indicated no bulk structural change. The Pb 4f and Te 3d peaks were observed at 138.7 and 576.4 eV and are significantly shifted from those of pure PbTe.[30] The position of Pb $4f_{7/2}$ corresponds to the expected chemical shifts for either $Pb(OH)_2$[31] or PbO.[32] The two strong peaks associated with Te 3d are a result of TeO_2 (Te^{IV}). This phenomenon can be attributed to Te being more metallic in character than its counterparts (S or Se). This correlation is in good agreement with a previous study.[30] Moreover, the presence of a high-binding phosphorus 2p signal at 133.1 eV is compatible with oxidized P-containing species.[33] This is consistent with the presence of TOPO (from oxidation of TOP), rather than phosphorus, from decomposition of the precursor (~130 eV).[10b,d] Carbon contamination in the film is also apparent, but the origin is uncertain. Although the precursor itself is a possible source, it could also occur during the handling of the films.

Conclusions

Sn^{II} and Pb^{II} complexes of symmetric and asymmetric tellurium-centered imidodiphosphinate ligands were synthesized and characterized by X-ray crystallography. In contrast to most related literature examples, the ditellurido complexes $M[(TeP^iPr_2)N]_2$ (**5**, M = Sn; **6**, M = Pb) were shown to be dimeric in the solid state through M···Te interactions to give square-pyramidal metal centers with a stereochemically active lone pair of electrons. The mixed-chalcogen complex $Pb(TeP^iPr_2NP^iPr_2Se)_2$ (**8**) also crystallized as a dimer: the chalcogen sites were disordered, but a slight preference for Pb···Te interactions was deduced. In contrast, the tin(II) analogue $Sn(TeP^iPr_2NP^iPr_2Se)_2$ (**7**) crystallized as a monomeric molecule with no chalcogen disorder, suggesting that the factors influencing the dimerization of these complexes in solution involve weak interactions easily influenced by crystal-packing forces.

Complex **6** was shown to be a suitable SSP for the synthesis of phase-pure PbTe via solvothermal techniques at temperatures as low as 200 °C. The injection technique leads to spontaneous growth of PbTe on a preheated substrate. This method provides an additional strategy for preparing PbTe particles at low temperatures and has the potential to be used for the controlled synthesis of PbTe nanocrystals via thermolysis in an appropriate solvent system.

Acknowledgment. We gratefully acknowledge financial support from the Natural Sciences and Engineering Research Council of Canada (T.C. and J.S.R.), Alberta Ingenuity (J.S.R.), the Izaak Walton Killam Memorial Foundation (J.S.R.). P.O.B. and M.A. thank the EPSRC of the U.K. for funding. We thank Dr. Dana J. Eisler for collecting single-crystal X-ray diffraction data for the complex **5**.

Supporting Information Available: CIF files giving crystallographic data and figures giving TGA/DTA plots for the complex **6** and XPS spectra for PbTe wires. This material is available free of charge via the Internet at http://pubs.acs.org.

(30) Grant, R. W.; Pasko, J. G.; Longo, J. T.; Andrews, A. M. *J. Vac. Sci. Technol.* **1976**, *13*, 940.
(31) Taylor, J. A.; Perry, D. L. *J. Vac. Sci. Technol., A* **1984**, *2*, 771.
(32) Nefedov, V. *Surf. Interface Anal.* **1980**, *2*, 171.
(33) Guzelian, A. A.; Katari, J. E. B.; Kadavanich, A. V.; Banin, U.; Hamad, K.; Juban, E.; Alivisatos, A. P.; Wolters, R. H.; Arnold, C. C.; Heath, J. R. *J. Phys. Chem.* **1996**, *100*, 7212.